Aqueous access pathways in subunit *a* of rotary ATP synthase extend to both sides of the membrane

Christine M. Angevine, Kelly A. G. Herold, and Robert H. Fillingame*
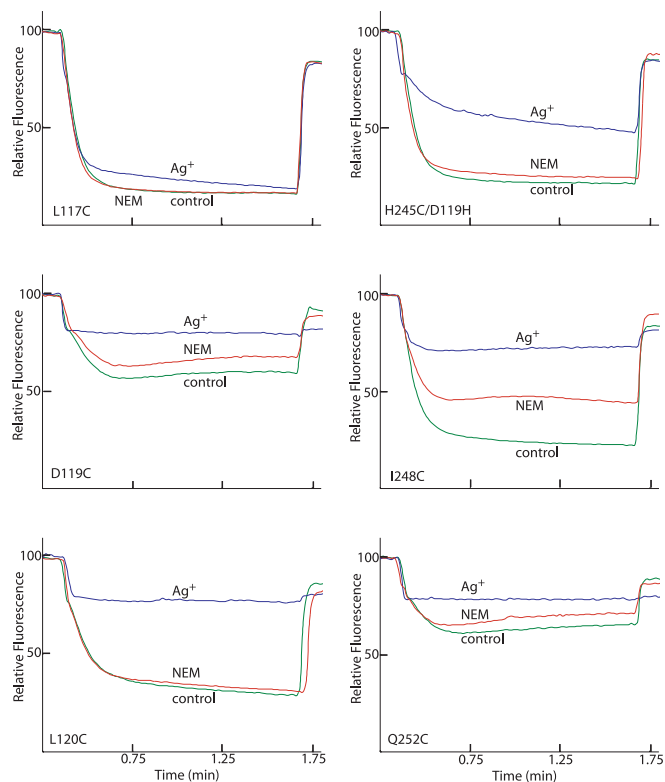
Department of Biomolecular Chemistry, University of Wisconsin Medical School, Madison, WI 53706

The role of subunit *a* in promoting proton translocation and rotary motion in the *Escherichia coli* F_1F_o ATP synthase is poorly understood. In the membrane-bound F_o sector of the enzyme, H^+ binding and release occur at Asp-61 in the middle of the second transmembrane helix (TMH) of subunit *c*. Protons are thought to reach Asp-61 at the center of the membrane via aqueous channels formed at least in part by one or more of the five TMHs of subunit *a*. Aqueous access pathways have previously been mapped to surfaces of *a*TMH4. Here we have substituted Cys into the second and fifth TMHs of subunit *a* and carried out chemical modification with Ag^+ and *N*-ethylmaleimide to define the aqueous accessibility of residues along these helices. Access to *c*Asp-61 at the center of the membrane may be mediated in part by Ag^+-sensitive residues 248, 249, 251, and 252 in *a*TMH5. From the periplasmic surface, aqueous access to *c*Asp-61 may be mediated by silver-sensitive residues 115, 116, 119, 120, 122, and 126 in *a*TMH2. The Ag^+-sensitive residues in TMH2, -4, and -5 form a continuum extending from the periplasmic to the cytoplasmic side of the membrane. In an arrangement of helices supported by second-site revertant and crosslinking analyses, these residues cluster at the interior of a four-helix bundle formed by TMH2–5. The aqueous access pathways at the interior of subunit *a* may be gated by a swiveling of helices in this bundle, alternately exposing cytoplasmic and periplasmic half channels to *c*Asp-61 during the H^+ transport cycle.

Fig. 1. Differing sensitivity of Cys substitutions in *a*TMH2 and *a*TMH4 to Ag^+ and NEM. A 160-μl aliquot of membranes at 10 mg/ml in TMG-acetate was treated with 5 mM NEM for 15 min at room temperature and then diluted into 3.2 ml of HMK buffer containing 0.3 μg/ml ACMA. Alternatively, membranes were diluted into HMK buffer and AgNO$_3$ added to 40 μM for 15 min at room temperature before addition of ACMA. ATP was added to 0.94 mM at 20 s, and the uncoupler nigericin was added to 0.5 μg/ml at 100 s. The traces indicate no treatment (green), NEM treatment (red), or Ag^+ treatment (blue). The substitution tested is indicated.

$\mathbf{H}^+$ transporting F_1F_o ATP synthases consist of two structurally and functionally distinct sectors termed F_1 and F_o. In the intact enzyme, ATP synthesis or hydrolysis takes place in the F_1 sector and is coupled to active H^+ transport through the F_o sector. Structurally similar F_1F_o ATP synthases are present in mitochondria, chloroplasts, and most eubacteria (1). The F_1 sector lies at the surface of the membrane and in *Escherichia coli* consists of five subunits in an $\alpha_3\beta_3\gamma_1\delta_1\epsilon_1$ stoichiometry. The F_o sector spans the membrane and in *E. coli* consists of three subunits in an $a_1b_2c_{10}$ stoichiometry (2). In the complete membranous enzyme, the rotation of subunit γ is proposed to be driven by H^+ transport-coupled rotation of a connected ring of *c* subunits in the F_o sector of the enzyme. The *c* subunit spans the membrane as a hairpin of two α-helices, and in the case of *E. coli*, contains the essential Asp-61 residue at the center of the second transmembrane helix (TMH). Asp-61 is thought to undergo protonation and deprotonation as each subunit of the oligomeric ring moves past a stationary subunit *a*. Subunit *a* is believed to provide access channels to the proton-binding Asp-61 residue, but the actual proton translocation pathway is only partially defined (3–5).

Subunit *a* is known to fold with five TMHs (6–8), with *a*TMH4 packing in parallel to *c*TMH2, i.e., the helix to which Asp-61 is anchored (9). The interaction of the conserved Arg-210 residue in *a*TMH4 with *c*TMH2 is thought to be critical during the deprotonation–protonation cycle of *c*Asp-61 (3, 4, 10–12). A number of studies support the positioning of subunit *a* and the two *b* subunits at the periphery of the *c* ring (3, 13, 14). Second-site revertant analysis (4, 6, 10, 15, 16) supports an

arrangement of helices with *a*TMH2 and *a*TMH5 in contact with *a*TMH4.

The chemical labeling of cysteine side chains introduced by site-directed mutagenesis has been used as a means of mapping aqueous accessible regions on many membrane proteins. Several reagents have been used to modify the genetically introduced Cys to determine accessibility, including *N*-ethylmaleimide (NEM) (17, 18) and Ag^+ (19). Modification of Cys by

---
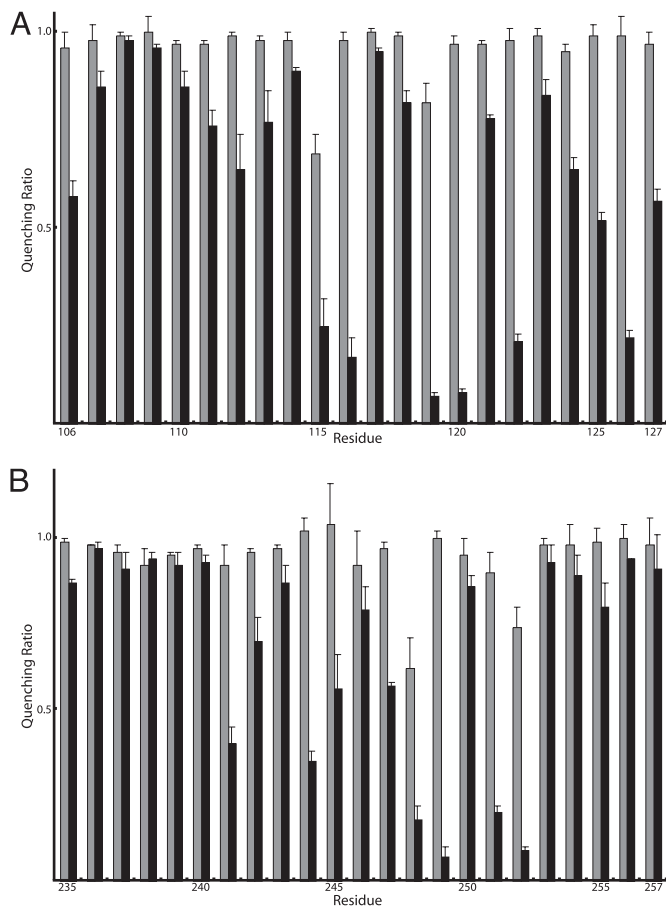
Fig. 2. NEM and Ag$^+$ sensitivity of residues in *a*TMH2 and *a*TMH5. Membranes were treated as described in the Fig. 1 legend. The results are presented as the ratios of quenching in the presence of Ag$^+$ or NEM to the quenching in the absence of either reagent. The gray bars represent the quenching ratio ± NEM treatment, and the black bars represent the quenching ratio ± Ag$^+$ treatment. Each bar represents the average ratio from $n \geq 2$ determinations ± SD. In nine trials of control membranes lacking Cys, quenching ratios of 0.96 ± 0.06 for NEM and 0.90 ± 0.04 for Ag$^+$ were observed relative to the untreated control.

these reagents is thought to depend on ionization of the Cys sulfhydryl to its thiolate form and thus is expected to occur preferentially in an aqueous environment (17–20). Previously, we used this method to test residues in *a*TMH4 for aqueous accessibility (5) and identified a silver-sensitive pocket centered around N214C in *a*TMH4 that extended to the cytoplasmic surface at Ser-206 and to residue H245C in TMH5 at the center of the membrane. In this report, we have focused on TMH2 and *a*TMH5, using the same methods, and these studies reveal two distinct regions of aqueous accessibility in subunit *a*. Cys substitutions in residues 115, 116, 119, 120, 122, and 126 of *a*TMH2 are very sensitive to Ag$^+$ and may probe an aqueous pathway from *c*Asp-61 to the periplasmic surface of the membrane. In *a*TMH5, Cys substitutions in residues 248, 249, 251, and 252 of *a*TMH5 are most sensitive to Ag$^+$ modification and appear to form an aqueous accessible pocket at the center of the membrane. Taken together, these results indicate that subunit *a* may facilitate aqueous access to *c*Asp-61 from both sides of the membrane. We propose that the swiveling of helices in subunit *a* may lead to the alternate exposure of the cytoplasmic and periplasmic half channels to *c*Asp-61 during the protonation–deprotonation cycle.
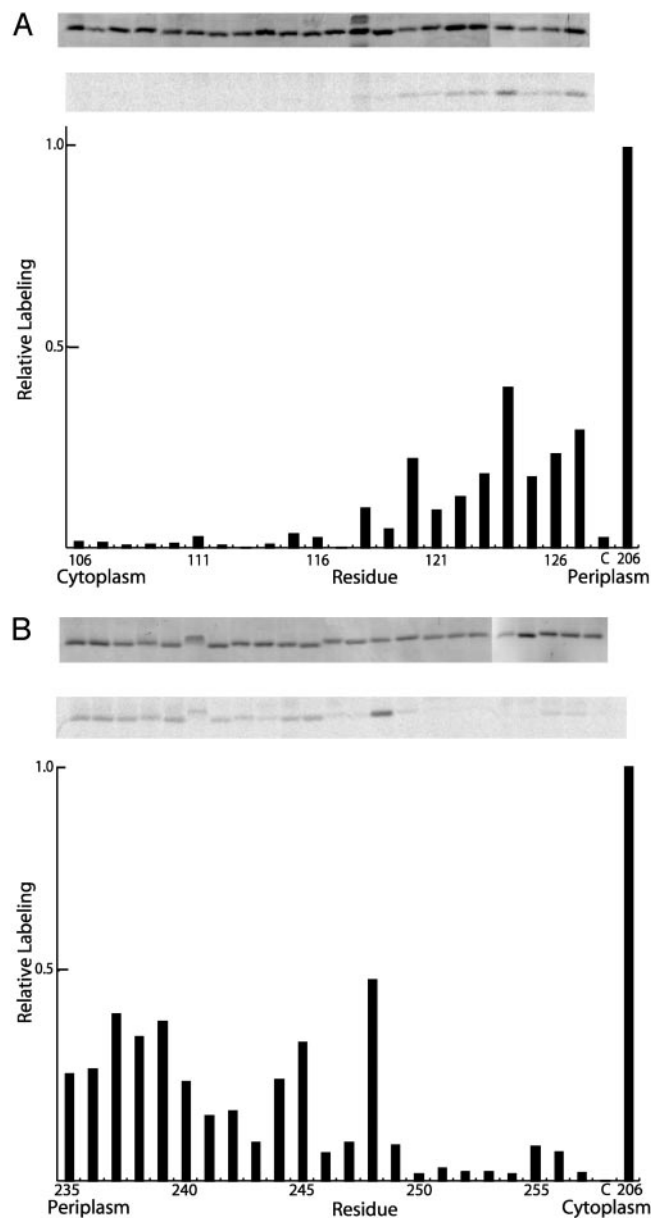
Fig. 3. Labeling of *a*TMH2 and *a*TMH5 with ^{14}C NEM. Membranes from various *a*TMH2 and *a*TMH5 mutants were treated at 10 mg/ml in TMG-acetate buffer (pH 7.5) with 1 mM ^{14}C NEM for 1 h at room temperature. The membranes were then solubilized with SDS, and subunit *a* was purified with nickel-nitrilotriacetic acid-agarose. Samples were subjected to SDS/PAGE, and the radioactivity in the dried gel was quantitated with a PhosphorImager. (*A*) *a*TMH2 data. (*B*) *a*TMH5 data. (*A* and *B Top*) Coomassie stain of dried gel, used to normalize the labeling intensities. (*A* and *B Middle*) PhosphorImage of dried gel. (*A* and *B Bottom*) Bar graph of labeling intensity normalized to Coomassie staining intensity. In all experiments, *a*S206C membranes were used as a positive control for labeling, and the labeling intensity for *a*S206C represents 100% on the bar graph. The C bar on the graphs represent labeling results for the control membranes lacking Cys in F_1F_o.

Experimental Procedures

Construction of Cys-Substituted Mutants. The cysteine substitutions generated here were transferred into plasmid pCMA113 (5), which contains a hexahistidine tag on the C terminus of subunit *a* (6) and genes encoding the entire *unc* (*atp*) operon in which all endogenous Cys had been substituted by Ala (21). Most cysteine substitutions were introduced by a two-step PCR method by using a synthetic oligonucleotide, which contained the codon
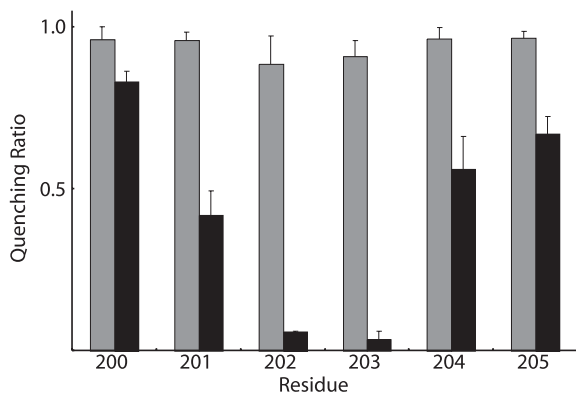
Fig. 4. NEM and Ag$^+$ sensitivity of residues at the cytoplasmic end of *a*TMH4. Membranes were treated as described in the legend to Fig. 1. The results are presented as the ratios of quenching in the presence of NEM or Ag$^+$ to the quenching in the absence of either reagent. The gray bars represent the quenching ratio ± NEM treatment, and the black bars represent the quenching ratio ± Ag$^+$ treatment. Each bar represents the average ratio from $n = 3$ determinations ± SD.

change, and two wild-type primers (22). *a*TMH5 PCR products were transferred directly into pCMA113 by using unique *Pfl*MI (1,136) and *Bsr*GI (1,913) sites (see ref. 23 for nucleotide numbering). *a*TMH2 products were transferred into pVF196 (6) by using *Nco*I (1,305) and *Pst*I (1,565) sites and then transferred to pCMA113 with *Hin*dIII and *Bsr*GI, as described above. All mutations were confirmed by sequencing the cloned fragment through the ligation sites. All experiments were performed with the mutant whole operon plasmid derivative of pCMA113 in the *unc* operon deletion host strain JWP292 (2). All plasmid transformant strains were tested for growth on succinate and glucose as described (5).

ATP-Driven Quenching of 9-Amino-6-chloro-2-methoxyacridine (ACMA) Fluorescence. Cells were grown and membranes prepared as described (5). Membranes were suspended in 3.2 ml of HMK

buffer [10 mM Hepes·KOH/1 mM Mg(NO$_3$)$_2$/10 mM KNO$_3$, pH 7.5] ACMA was added to a 0.3 μg/ml final concentration, and 30 μl of 0.1 M ATP, pH 7.0, was added to initiate quenching of fluorescence. The reaction was terminated by addition of 8 μl of 288 μM nigericin (0.5 μg/ml final concentration). The level of fluorescence obtained after addition of nigericin was normalized to 100% in calculating the percent quenching due to ATP-driven proton pumping (Table 1). For AgNO$_3$ treatment, 160 μl of membranes at 10 mg/ml was suspended in HMK buffer containing 40 μM AgNO$_3$ and incubated at room temperature for 15 min before carrying out the quenching assay. For NEM treatment, membranes were pretreated at 10 mg/ml in TMG-acetate buffer (50 mM Tris-acetate/5 mM magnesium acetate/10% glycerol, pH 7.5) with 5 mM NEM, and then diluted into HMK-nitrate buffer before carrying out the same quenching assay.

[^{14}C]*N*-ethylmaleimide Labeling Studies. ^{14}C-NEM (New England Nuclear, 34.2 mCi/mmol) in pentane was added to TMG-acetate buffer and the pentane evaporated by blowing a stream of argon over the solution. The resulting aqueous solution of NEM was then added to 3 mg of membrane vesicles in TMG-acetate buffer such that the final concentration of membranes was 10 mg/ml, and the final concentration of ^{14}C-NEM was 1 mM. The mixture was incubated at room temperature for 1 h, after which the reaction was stopped by addition of 2-mercaptoethanol to 10 mM. SDS was added to 1% and unlabeled NEM to 20 mM. His-tagged subunit *a* was purified from the SDS-solubilized membranes as described (5). Subunit *a* purified from 1 mg of membranes was analyzed by SDS/PAGE on a 12% Tris-tricine gel (24), and the resulting gel was stained with Coomassie blue and dried. The intensity of staining of all bands shown falls within the linear range for this dye. The dried gel was exposed to a storage phosphor screen and scanned with a PhosphorImager (Molecular Dynamics) to quantitate radioactivity incorporated into the subunit *a* band. To determine the amount of protein in each band, the stained dried gel was scanned by using a flatbed scanner linked to a Macintosh computer with TWAIN 5 software (Epson,
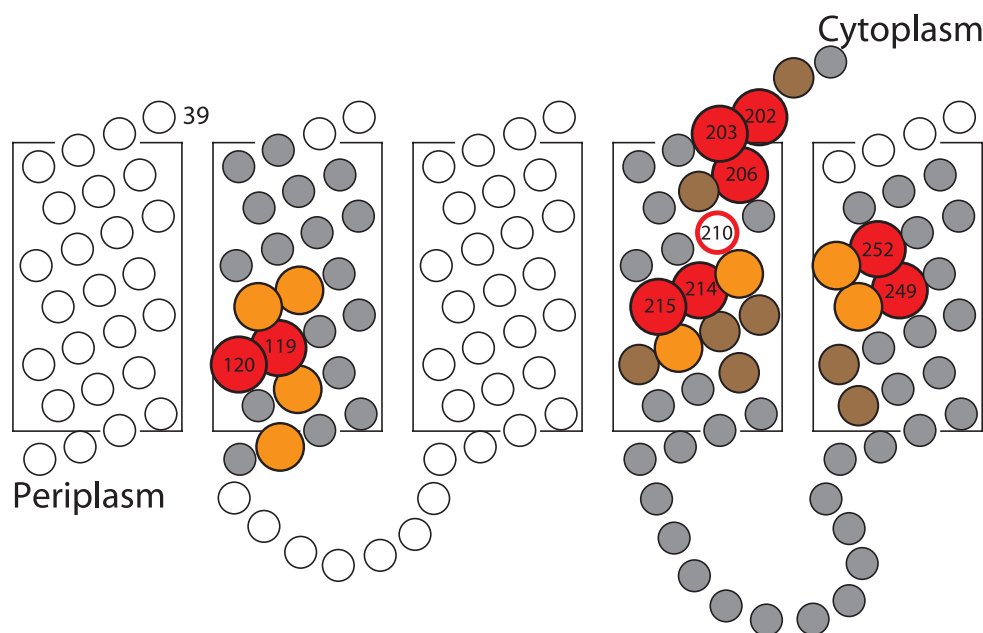
Fig. 5. Ag$^+$-sensitive residues represented in a 2D topological model. Residues that are most sensitive to modification by Ag$^+$ are shown in red (>90% inhibition), orange (76–90% inhibition), and brown (50–75% inhibition). Less-sensitive and insensitive residues are shown in gray, and untested residues are white.

Long Beach, CA). The scan was quantitated by using the public domain NIH IMAGE program.[†]

Results

Cys Substitutions in TMH2 and *a*TMH5 of Subunit *a*. In this study, Cys substitutions in the second and fifth TMHs of subunit *a* were transferred into a His-tagged version of subunit *a* in a plasmid that coded the entire *unc* (*atp*) operon wherein all of the endogenous Cys in F_1 and F_o had been substituted by Ala (5). These plasmids were transformed into JWP292, a strain with a chromosomal deletion of the entire *unc* operon. The transformant strains were tested for growth yield on glucose and relative colony size on succinate-containing minimal medium. The Cys substitutions in TMH2 and -5 of subunit *a* reported here had little effect on growth (see Table 1, which is published as supporting information on the PNAS web site). Additionally, ATP-driven quenching of ACMA fluorescence was performed on inside-out membrane vesicles of the substituted strains to evaluate ATPase-coupled H^+ pumping function (Table 1). Of the 45 mutants tested, only D119C in TMH2 and Q252C in TMH5 exhibited substantial reductions in the quenching response (Fig. 1).

Inhibition of ATPase-Coupled H^+ Transport by NEM or Ag^+ in *a*TMH2. Inside-out membrane vesicles with Cys substitutions in residues 106–127 were treated with 5 mM NEM or 40 μM AgNO$_3$ in chloride-free assay buffer, and ATPase-coupled H^+ transport was measured by the quenching of ACMA fluorescence. Representative quenching traces for several mutants are presented in Fig. 1. NEM had negligible inhibitory effects on all Cys substitutions in *a*TMH2, as summarized in Fig. 2*A*. In contrast, Ag^+ inhibited quenching markedly in several of the mutants tested, including Cys substitutions at residues 115, 116, 119, 120, 122, and 126 (Fig. 2*A*).

Inhibition of ATPase-Coupled H^+ Transport by NEM or Ag^+ in *a*TMH5. Inside-out membrane vesicles with Cys substitutions in residues 235–257 of the putative *a*TMH5 and residues 225–234 of the likely periplasmic loop between *a*TMH4 and *a*TMH5 were tested for NEM and Ag^+ inhibition of ATP-driven ACMA quenching. NEM had little inhibitory effect on any of the 33 residues tested, showing very modest inhibition with only residues 248 and 252 (Figs. 1 and 2*B*). However, as with *a*TMH2, a number of mutants were inhibited by Ag^+ treatment, the most sensitive being 248, 249, 251, and 252, with other mutants including 241, 244, 245, and 247 showing lesser sensitivity (Fig. 2*B*).[‡]

^{14}C-NEM Labeling of Cys in *a*TMH2 and *a*TMH5. To check whether NEM reacted with residues in the suggested transmembrane regions without causing inhibition of quenching, inside-out membrane vesicles from the *a*TMH2 and *a*TMH5 mutants were treated with 1 mM ^{14}C-NEM for 1 h. The hexahistidine-tagged subunit *a* was then purified by Ni^{+2} affinity chromatography, and the amount of label incorporated into subunit *a* was quantified by Phosphor-Image analysis. Of the 45 substitutions tested, only residues 244, 245, and 248 at the center of *a*TMH5 were labeled moderately relative to the most NEM-sensitive control, Cys-206 in *a*TMH4.[§] Other substitutions showing moderate labeling clustered at the

periplasmic sides or in extramembranous loops at the ends of both *a*TMH2 and *a*TMH5 (Fig. 3 *A* and *B*). Residues at the cytoplasmic sides of the helices showed little or no labeling.
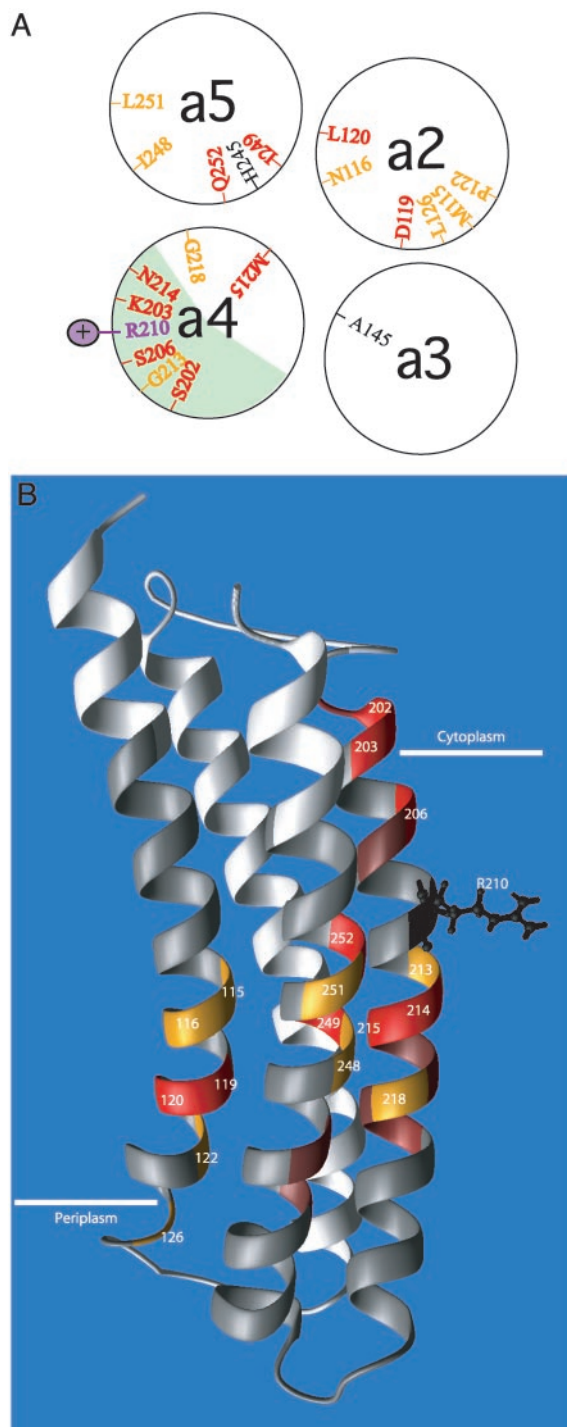
Fig. 6. Two distinct regions of Ag^+ sensitivity in subunit *a*. (*A*) Cross-sectional view of TMH2–5 of subunit *a* depicted as α-helical wheels. The most Ag^+-sensitive residues are shown in red (>90% inhibition) and orange (76–90% inhibition). The position of the *a*Arg-210 side chain is also indicated. The light green area on *a*TMH4 represents the helical face that crosslinks to TMH2 of subunit *c*. (*B*) Placement of Ag^+-sensitive residues in 3D model of subunit *a* by Rastogi and Girvin (25) (Protein Data Bank entry 1C17). Ag^+-sensitive residues are indicated as described in Fig. 5, i.e., red (>90% inhibition), orange (76–90% inhibition), and brown (50–75% inhibition). Insensitive residues are shown in gray, and untested residues are white.

[‡]We previously reported that the *a*H245C/D119H mutant membranes, which were made partially functional by the D119H second-site suppressor, were inhibited by ≈50% by 40 μM Ag^+ and nearly completely by 80 μM Ag^+. The membranes used here were expressed from a plasmid carrying the complete *unc* operon, vs. the partial operon plasmid used previously, and expressed with an F_1 containing no Cys. These differences likely account for the quite robust activity and slightly reduced Ag^+ sensitivity observed here.

[§]The ^{14}C-NEM labeling of *a*I248C shown in Fig. 3*B* appears more extensive than would be predicted from the 38% inhibition shown in Fig. 2*B* and Table 1. The discrepancy may be due to differences in the conditions used for labeling with ^{14}C-NEM vs. that for inhibition of ATP-driven quenching (see *Experimental Procedures*).

Ag⁺-Sensitive Residues at the Cytoplasmic End of *a*TMH4. Cys substitutions in *a*TMH4 had previously been tested for Ag⁺ and NEM sensitivity over the span of residues 206–224 (5). The relative Ag⁺ and NEM sensitivity of residues 200–205 is shown in Fig. 4. Although NEM-insensitive, residues 202 and 203 proved to be extremely sensitive to inhibition by Ag⁺. Therefore, it appears that the pattern of Ag⁺-sensitive residues on one helical face of *a*TMH4 extends from N214C at the center of the membrane to residues S202C, K203C, and S206C at or near the cytoplasmic surface.

Discussion

Here we report experiments defining aqueous accessible residues in the second and fifth TMHs in subunit *a* of the rotary ATP synthase. Previously, we had reported on the aqueous accessibility of residues in *a*TMH4 (5). Several second-site revertants support an arrangement of TMHs with *a*TMH2 and *a*TMH5 in contact with *a*TMH4 (4, 6, 10, 15, 16). Such an arrangement is now supported by crosslinking between the helical pairs of *a*TMH2/TMH4, *a*TMH2/TMH5, and *a*TMH4/TMH5 (B. Schwem and R.H.F., unpublished work). The results presented here support the idea that all three helices form parts of the aqueous access pathway to Asp-61 of subunit *c*. Very few of the residues reported here are sensitive to inhibition by NEM. This may be due to the restricted size of the pathway through which protons reach *c*Asp-61. The small size of the Ag⁺ ion, relative to the bulkier NEM, may make it an ideal probe of the aqueous access pathways in subunit *a*.

The positions of Ag⁺-sensitive residues in TMH2, -4, and -5 are shown in a 2D topological representation of subunit *a* in Fig. 5. *a*TMH2 appears to provide an aqueous pathway leading from the periplasm to the center of the membrane, whereas Ag⁺-sensitive residues in *a*TMH4 extend from the center of the membrane to the cytoplasmic surface. The most Ag⁺-sensitive residues in *a*TMH5 cluster at the center of the membrane and extend toward the periplasmic surface. When TMH2, -4, and -5 are brought into juxtaposition, they may form an aqueous cavity at the center of the membrane, which would locate primarily to the center of the modeled four-helix bundle (Fig. 6*A*). A 3D representation of the four-helix bundle is shown in Fig. 6*B*. From inspection of Fig. 6*A*, it is apparent that there are two distinct regions of silver sensitivity in subunit *a*. The first region is the face of *a*TMH4 that crosslinks with *c*TMH2. This is also the most NEM-sensitive region, NEM reactivity extending from residue 214 at the center of the membrane to residue 206 at the cytoplasmic surface. Other regions of Ag⁺-sensitive residues cluster toward the interior of the four-helix bundle modeled for subunit *a*. The clustering of Ag⁺-sensitive residues at the center of the four-helix bundle raises the question of how protons in such an aqueous accessible pocket would reach Asp-61 of subunit *c*. It therefore seems likely that movement and repositioning of these helices may be necessary during the course of the proton transport cycle, as discussed below.

We have previously proposed a model for rotary function in which the concerted swiveling of helices within the four-helix bundle of subunit *a* may provide a mechanism of gating alternate access of protons to *c*Asp-61, and in turn be linked to the mechanical movements driving *c*-ring rotation (4). In the model, the H⁺-transport cycle is initiated by the swiveling of TMH2 of subunit *c*, bringing *c*Asp-61 and *a*Arg-210 in juxtaposition and simultaneously aligning the helical faces of *c*TMH2 and *a*TMH4 in the position required for crosslinking (9). After deprotonation of *c*Asp-61 and exit of the proton to the cytoplasm via the *a*S206C NEM-sensitive channel, the helices of subunit *a* are proposed to swivel in a concerted fashion to move *a*Arg-210 away from *c*Asp-61 to facilitate its reprotonation, and simultaneously gate movement of protons from the periplasmic channel centered in the four-helix bundle. After protonation of *c*Asp-61, the helices are proposed to swivel against each other to return to their original position, and in a manner akin to meshed gears, drive the stepwise rotation of the *c*-rotor. The mapping of Ag⁺-sensitive residues (presumed to reflect aqueous access) to the interior of the proposed four-helix bundle lends support to a model of this type and immediately predicts that aqueous exposure of different regions of the protein should change during the H⁺-transport cycle. We expect that this prediction can be tested in future experiments.

1. Senior, A. E. (1988) *Physiol. Rev.* **68,** 177–231.
2. Jiang, W., Hermolin, J. & Fillingame, R. H. (2001) *Proc. Natl. Acad. Sci. USA* **98,** 4966–4971.
3. Cain, B. D. (2000) *J. Bioenerg. Biomembrane* **32,** 365–371.
4. Fillingame, R., Angevine, C. & Dmitriev, O. (2002) *Biochim. Biophys. Acta* **1555,** 29–36.
5. Angevine, C. M. & Fillingame, R. H. (2003) *J. Biol. Chem.* **278,** 6066–6074.
6. Valiyaveetil, F. I. & Fillingame, R. H. (1998) *J. Biol. Chem.* **273,** 16241–16247.
7. Long, J. C., Wang, S. & Vik, S. B. (1998) *J. Biol. Chem.* **273,** 16235–16240.
8. Wada, T., Long, J. C., Zhang, D. & Vik, S. B. (1999) *J. Biol. Chem.* **274,** 17353–17357.
9. Jiang, W. & Fillingame, R. H. (1998) *Proc. Natl. Acad. Sci. USA* **95,** 6607–6612.
10. Hatch, L. P., Cox, G. B. & Howitt, S. M. (1995) *J. Biol. Chem.* **270,** 29407–29412.
11. Valiyaveetil, F. I. & Fillingame, R. H. (1997) *J. Biol. Chem.* **272,** 32635–32641.
12. Fillingame, R. H. (1990) in *The Bacteria,* ed. Krulwich, T. A. (Academic, New York), Vol. XII, pp. 345–391.
13. Dunn, S. D., McLachlin, D. T. & Revington, M. (2000) *Biochim. Biophys. Acta* **1458,** 356–363.
14. Jones, P. C., Hermolin, J., Jiang, W. & Fillingame, R. H. (2000) *J. Biol. Chem.* **275,** 31340–31346.
15. Cain, B. D. & Simoni, R. D. (1988) *J. Biol. Chem.* **263,** 6606–6612.
16. Hartzog, P. E. & Cain, B. D. (1994) *J. Biol. Chem.* **269,** 32313–32317.
17. Tamura, N., Konishi, S., Iwaki, S., Kimura-Someya, T., Nada, S. & Yamaguchi, A. (2001) *J. Biol. Chem.* **276,** 20330–20339.
18. Mordoch, S. S., Granot, D., Lebendiker, M. & Schuldiner, S. (1999) *J. Biol. Chem.* **274,** 19480–19486.
19. Lu, Q. & Miller, C. (1995) *Science* **268,** 304–307.
20. Li, J., Xu, Q., Cortes, D. M., Perozo, E., Laskey, A. & Karlin, A. (2002) *Proc. Natl. Acad. Sci. USA* **99,** 11605–11610.
21. Kuo, P. H., Ketchum, C. J. & Nakamoto, R. K. (1998) *FEBS Lett.* **426,** 217–220.
22. Barik, S. (1996) *Methods Mol. Biol.* **57,** 203–215.
23. Gay, N. J. & Walker, J. E. (1981) *Nucleic Acids Res.* **9,** 2187–2194.
24. Schagger, H. & von Jagow, G. (1987) *Anal. Biochem.* **166,** 368–379.
25. Rastogi, V. K. & Girvin, M. E. (1999) *Nature* **402,** 263–268.

BIOCHEMISTRY